A Novel Fault Indicator for Local Demagnetization in Fractional-Slot Permanent Magnet Synchronous Motor using Winding Function Theory

Milad Golzar[1, 2], Surya Teja Kandukuri[1], Van Khang Huynh[1], Martin Marie Hubert Choux[1], Alf Magne Midtbø Versland[2]

[1]*Department of Engineering Sciences, University of Agder, Grimstad, Norway*

milad.golzar@uia.no
surya.kandukuri@uia.no
huynh.khang@uia.no
martin.choux@uia.no

[2] *Flekkefjord Elektro Ltd., 4400 Flekkefjord, Norway*

amm@felektro.no

ABSTRACT

Local demagnetization is an irreparable failure mode in permanent magnet synchronous motors (PMSMs), resulting in reduced motor efficiency and high cogging torque. These effects are particularly disadvantageous to fractional-slot wound PMSMs used in industrial applications, such as robotics and automations, that require high power density and precise operation. In this article, a diagnostic indicator is developed for detecting local demagnetization fault in fractional-slot wound PMSMs based on winding function theory, utilizing back-electromotive force (back-EMF) as a medium for fault detection. Further, the developed indicator is validated in a commercial fractional-slot wound PMSM of an in-house experimental setup.

1. INTRODUCTION

Fractional-slot PMSMs are widely used in a variety of applications, including the automobile industry, automation, and robotics due to high power density, low cogging torque, and torque ripple (Hendershot & Miller, 2010). Faults in PMSMs, especially local demagnetization, can lead to a reduction in efficiency and precision. Therefore, early detection of such anomalies in the PMSMs is a necessity for these applications (Faiz & Mazaheri-Tehrani, 2017). Winding function theory (WFT) and modified winding function theory (MWFT) have been developed for fault diagnosis in induction machines (Toliyat, Nandi, Choi, & Meshgin-Kelk, 2012). The WFT is computationally cheaper than finite element method (FEM) and proven to be comparable in accuracy to FEM (Ilamparithi & Nandi, 2010). Within this work, this approach is further developed to detect faults in the fractional-slot wound PMSMs.

In recent years, rotor demagnetization of PMSM has gained a great attention in literature (Naderi, 2018; Park, Fernandez, Lee, Hyun, Jeong, Kommuri, Cho, Diaz Reigosa & Briz, 2019; Usman, Joshi & Rajpurohit, 2019). A PMSM with trapezoidal back electromotive force (back-EMF) under healthy and faulty conditions was modeled using combined FEM and analytical approach (Usman et al., 2019). Faults in surface-mounted PMSM with symmetrical stator windings were analyzed using FEM and experimental tests by Urresty, Riba, and Romeral (2013). Moon, Lee, Jeong, and Kim (2016) studied the demagnetization fault via structural analysis of inductances of PMSM under stationary and non-stationary conditions. The demagnetization fault of PMSM was detected using analog Hall effect sensors by Park et al. (2019). Faiz and Nejadi-Koti (2016) summarized available fault indexes for demagnetization fault in PMSMs. However, to the authors' knowledge, analysis of faults in fractional-slot wound PMSMs has not been mentioned in the literature. In this article, we demonstrate that the back-EMF in fractional-slot PMSMs can be used as a reliable diagnostic indicator. The proposed method is validated by a laboratory setup, using a commercial PMSM.

This paper is organized as follows. Section two describes the theoretical background based on WFT for detecting local demagnetization in PMSMs. The laboratory setup and associated results are detailed in Section three. Finally, the paper is concluded in Section four.

2. WINDING FUNCTION THEORY

The WFT utilizes a so-called winding function to calculate the phase winding inductances (L) and flux linkages (λ) (Lipo, 2017). The PMSM voltage equation can be represented in the a-b-c stationary reference frame as

$$v(t) = r_s i(t) + \frac{d\lambda}{dt} \tag{1}$$

where v , i and λ are the three-phase voltages, currents, and flux linkages and r_s is the stator phase winding resistance matrix, which are detailed as below

$$v^T = \begin{bmatrix} v_a & v_b & v_c \end{bmatrix} \tag{2}$$

$$i^T = \begin{bmatrix} i_a & i_b & i_c \end{bmatrix} \tag{3}$$

$$\lambda^T = \begin{bmatrix} \lambda_a & \lambda_b & \lambda_c \end{bmatrix} \tag{4}$$

$$r_s = \begin{bmatrix} r_a & 0 & 0 \\ 0 & r_b & 0 \\ 0 & 0 & r_c \end{bmatrix} \tag{5}$$

The phase winding flux $\lambda_{i,i=a,b,c}$ and stator self and mutual inductances are derived as follows (Lipo, 2017)

$$\lambda_i = \sum_{j=1}^{WindingNo} \lambda_{ij} + \lambda_{i-mag} \tag{6}$$

and

$$L_{ij} = \frac{\lambda_{ij}}{i_j} = \int_0^{2\pi} n_i(\varphi) N_j(\varphi) \rho(\varphi) d\varphi \tag{7}$$

where λ_{ij} , λ_{i-mag} , $\rho(\varphi)$, $n_i(\varphi)$ and $N_j(\varphi)$ *(i, j = a, b, c)* are the winding fluxes produced by windings and magnets, permeance function, turns and winding function, respectively. The winding function $N_j(\phi)$ is defined as

$$N_j(\varphi) = n_j(\varphi) - \left\langle n_j(\varphi) \right\rangle \tag{8}$$

where $n_j(\phi)$ is the turns function and

$$\left\langle n_j(\varphi) \right\rangle = \frac{1}{2\pi \left\langle g^{-1}(\varphi) \right\rangle} \int_0^{2\pi} \frac{n_j(\varphi)}{g(\varphi)} d\varphi \tag{9}$$

is the mean of turns function (Lipo, 2017). Variable $g(\varphi)$ represents the electrical motor air gap. The turns function is equivalent to the total number of conductors in the slots at any arbitrary angle *($0 < \varphi < 2\pi$)* with respect to a reference point (φ = 0), around the periphery of the stator. This quantity, by definition, increases when passing a conductor carrying current out of the page, and vice versa. The winding magnetic flux due to magnets (λ_{i-mag}) can be calculated as

$$\lambda_{i-mag} = \int_0^{2\pi} n_i(\varphi) F_{mag}(\varphi, \theta) \rho(\varphi) d\varphi \tag{10}$$

where $F_{mag}(\varphi, \theta)$ is the so-called magnet function (Saied, Abbaszadeh, & Tenconi, 2011). This quantity is equivalent to the resultant zero-average magnetomotive force (MMF) from the magnets, and rotates by the angle of θ (rotor angular motion). $F_{mag}(\varphi, \theta)$ can be obtained as follows

$$F_{mag}(\varphi, \theta) = MMF_{mag}(\varphi, \theta) - \frac{1}{2\pi \left\langle g^{-1}(\varphi) \right\rangle} \int_0^{2\pi} \frac{MMF_{mag}(\varphi, \theta)}{g(\varphi)} d\varphi \tag{11}$$

where $MMF_{mag}(\varphi, \theta)$ represents the permanent magnet (PM) magnetomotive force. For a uniform magnet with a constant thickness (l_m) and magnetic field intensity (H_m), the $MMF_{mag}(\varphi, \theta)$ can be ideally determined by

$$MMF_{mag}(\varphi, \theta) = \begin{cases} H_m l_m & Magnetized\_Area \\ 0 & other \end{cases} \tag{12}$$

Both the winding functions and simplified magnetic function can be reproduced by the following Fourier series transform (FT)

$$F(x) = \frac{a_0}{2} + \sum_{n=1}^{K} \left(a_n \cos\left(\frac{2\pi n x}{P}\right) + b_n \sin\left(\frac{2\pi n x}{P}\right) \right) \tag{13}$$

where P is the period of the intended function, and K is the number of terms, which is an infinite integer. The winding magnetic fluxes can be obtained by substituting the respective transformations into Eqs. (10), (7), and (6). Then, the back-EMF voltages, i.e., open-circuit voltages, are calculated using Eq. (1). The accuracy of the resultant waveforms increases by considering a higher number of terms in the Fourier series approximation. According to Eq. (13), the higher-order terms add high-frequency sinusoid into the calculations. However, considering the computational burden, one may use a lower number of coefficients. The winding and simplified normalized magnet functions of the intended PMSM are shown in Figures 1 and 2. Concerning the mathematical simplification, the PM magnetomotive

force shown in Figure 2 is an approximated version of its practical values, having a square wave shape. Its shape roughly emulates the real MMF waveform of a surface-mounted PMSM with radially magnetized PMs, ignoring the fringing effect (Chen, Hu, Chen, & Peng, 2016). The presented MMF, however, is normalized, and a constant gain is required to modulate the calculated back-EMF voltages to match with its empirical values. In addition, the MMF of a specific case of partial demagnetization, equivalent to actual 15% demagnetization on one magnetic pole of the examined PMSM, is illustrated in Figure 2. This quantity is obtained by the summation of illustrated healthy and the hypothetical fault terms. Utilizing this fictitious MMF term, the implementation and modeling of different demagnetization fault conditions become simpler and modular.

2.1. Local Demagnetization Modeling

In this sub-section, the effect of local demagnetization on the motor back-EMF is analyzed using WFT. The turn function can be rewritten from Eq. (8) as

$$n_i(\varphi) = N_i(\varphi) + \langle n_i(\varphi) \rangle \tag{14}$$

where $\langle n_i(\varphi) \rangle$ is a constant, representing the turn function average value. Following the procedure mentioned earlier in this section, using trigonometric rules and simplifications, the stator winding magnetic fluxes for the healthy and hypothetical MMFs are obtained by substituting the Eq. (14) in Eq. (10) as

$$\lambda_{i-mag,H} = \sum_{h=1(odd)}^{K} (d_h a_{4h} \sin(4h\theta_{rm}) + d_h b_{4h} \cos(4h\theta_{rm})) \tag{15}$$

and

$$\lambda_{i-mag,F} = G_{demag} \sum_{h=1(odd)}^{K} ((e_h a_h \cos(h\theta_{rm}) + e_h b_h \sin(h\theta_{rm}) - f_h a_h \cos(h\theta_{rm}) + f_h b_h \cos(h\theta_{rm})) \tag{16}$$

where a_h, b_h are the Fourier series coefficients of the PMSM stator winding function. d_h, e_h and f_h are the corresponding coefficients of the healthy and fictitious permanent magnet MMFs. G_{demag} is the scalar value representing the demagnetization level of the rotor pole ($0 < G_{demag} < 1$). The resultant faulty magnetic flux can be calculated by the superimposition of Eqs. 15 and 16. It should be noted that, for the easier visualization in the time domain, the back-EMF of the motor with a 100% demagnetized pole is obtained. The back-EMF waveforms for both healthy and faulty PMSM are shown in Figure 3. The overall voltage amplitude is reduced, as in the case of motors with a symmetrical winding configuration having an integer number of slots per number of poles (Urresty, Riba, & Romeral, 2013). However, there is an additional amplitude change that occurs every four cycles and could be used as a reliable fault indicator. This is linked to the asymmetrical phase winding distribution of the studied fractional-slot PMSM shown in Figure 1. The frequency spectrums of the simulated back-EMF for healthy and faulty (fully demagnetized pole) conditions at 1000 rpm are illustrated in Figure 4. It is worth mentioning that similar fault frequencies might also appear in the frequency spectrum of PMSM having an asymmetrical airgap (rotor eccentricity). This could potentially degrade the performance of PMSM demagnetization fault diagnosis since the asymmetrical MMF and variable airgap length (permeance) have a similar effect in the airgap flux density, which should be carefully analyzed (Rajagopalan, Roux, Habetler, & Harley, 2007). However, a combination of voltage, current and estimation of magnetic strength were shown to produce improved distinguishability among several PMSM faults (Le Roux, Harley, & Habetler, 2003). These factors for the fractional-slot PMSMs will be investigated in further studies.

2.2. Diagnostic metric

To automate the process of diagnostics, it is necessary to formulate a diagnostic marker, which can detect changes in the current due to demagnetization. However, to detect the fault, such a marker needs to be unique. In the case of stator electrical faults, the extend Park's vector modulus (EPVM)

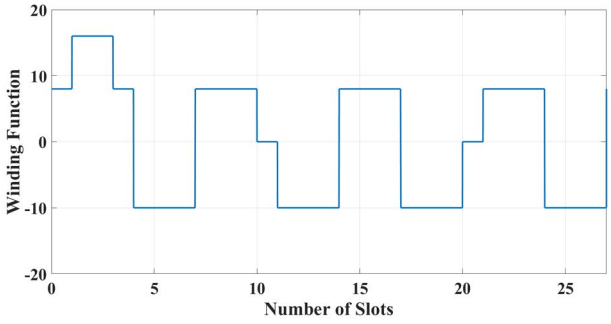

Fig. 1. The Winding function of examined fractional-slot PMSM.

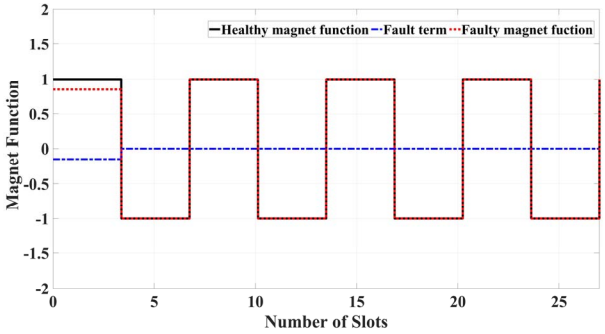

Fig. 2. Normalized Magnet function of the PMSM rotor.

on three-phase currents provides a unique marker in both synchronous and asynchronous machines (Cruz & Cardoso, 2001). However, to the authors' knowledge, a diagnostic metric for the case of demagnetization of fractional-slot wound motor does not exist in the literature. Based on the spectral analysis of back EMF as shown in Figure 4, a diagnostic metric is formulated based on the magnitude of the corresponding fault frequency as given by

$$D_m = \sum_{i=1}^{m} mag(f_{demag}) \tag{17}$$

where

$$f_{demag} = \frac{n}{4} f_s, n = 1,2,3,... \tag{18}$$

Since the harmonics of $f_s/4$ are observed in the spectrum, the supply frequency can be notch filtered before calculating D_m, being easily removed from the FFT spectrum. The calculated diagnostic metric is compared between the healthy and faulty conditions. The $D_m(Faulty)$ is found to be greater than $D_m(Healthy)$ by 250% in this case with a complete local demagnetization.

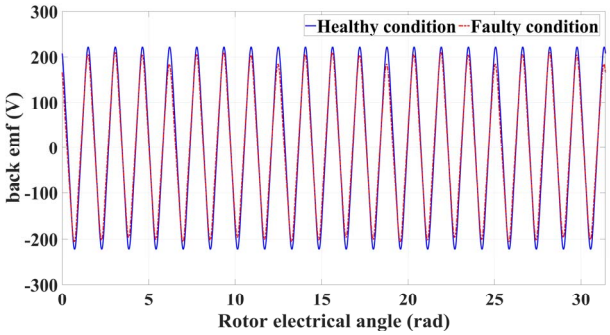

Fig. 3. The back-EMFs of the healthy and faulty PMSM at 1000rpm.

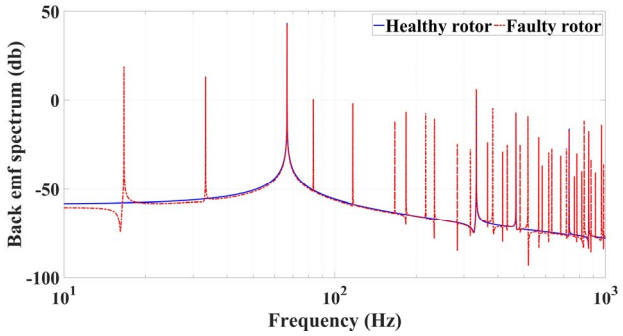

Fig. 4. The frequency spectrum of the simulated back-EMF at 1000rpm.

3. EXPERIMENTAL RESULTS

Experimental tests have been conducted to evaluate the accuracy of the winding function model and the proposed fault indicator under healthy and faulty condition on a fractional-slot PMSM, whose electrical specifications are given in the Table 1. Usually, PMSMs are demagnetized by removing and grinding part of the magnet (Urresty et al., 2013). This approach results in a mechanically imbalance rotor and introduces additional harmonics in the measurement. This then requires additional preprocessing and pre-analysis steps in order to distinguish between the harmonics caused due to mechanical imbalance and local demagnetization. In this work, electric discharge machine (EDM) is used to locally and partially demagnetize one pole. This method helps to keep almost all the magnetic materials in place while losing their magnetic strength, therefore better imitates the actual demagnetization in the PMSMs. The average magnetic strength of the faulty pole is reduced by 15% as measured by magnetometer over the entire pole surface. Figure 5 illustrates the laboratory setup and corresponding fractional-slot PMSMs. The motor under test is driven by a similar PMSM, which is controlled via a commercial drive with field-oriented control.

The back-EMF data is sampled by the time intervals of 2 μs and for the duration of 0.2 seconds. The rotor angular speed is set to 2400 rpm, which corresponds to 160 Hz electrical frequency in the stator windings and line-to-line back-EMF voltage of 363 volts (V_{LL_rms}). The spectrum of the analytical and experimental back-EMFs is shown in Figure 6. The frequency content in the back-EMF observed in the simulations matches that of the experimental results.

The supply frequency is 160 Hz. The dominant fault frequency appears at one-quarter of the fundamental frequency, i.e., 40 Hz. The presence of this sub-harmonic fault frequency is linked to the asymmetrical winding of the studied fractional-slot surface-mounted PMSMs, which could be monitored to detect the demagnetization fault and its severity. The experiments are repeated in healthy and

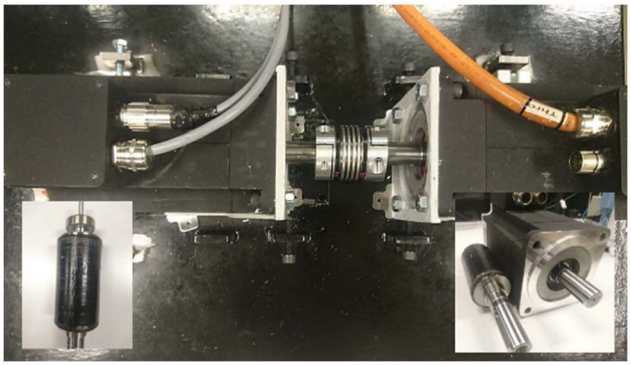

Fig. 5. Laboratory setup and corresponding fractional-slot PMSMs

Table 1. Parameters of the studied SPMSM.

Parameter	Value (unit)
Rated power	2.54 (kW)
Rated Speed	2400 (rpm)
Pole pairs	4
No. of stator slots	27
Back-emf at 1000 rpm	154.9 (V_{rms})
Magnet type	NdFeB

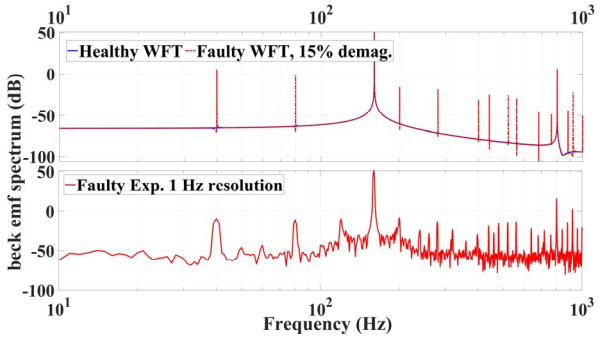

Fig. 6. The frequency spectrum of the modeled and measured back-EMFs for the rated speed of 2400 rpm.

faulty conditions and the diagnostic metric $D_m(Faulty)$ as described in Eq. (17), is calculated. It was found that the $D_m(Faulty)$ is greater than $D_m(Faulty)$ by 168% due to the partial local demagnetization.

4. CONCLUSION

In this paper, a diagnostic indicator is developed for local demagnetization in fractional slot wound PMSMs based on winding function theory. The results show that sub-harmonics in the spectral analysis of back-EMF could be used as a reliable indicator for local demagnetization fault. Despite the simplification in winding and magnet functions, the developed indicator using WFT is validated in a commercial fractional slot wound PMSM. The modeling based on WFT shown to be an appropriate and fast tool to model the imperfections and faults like the studied demagnetization. Although the diagnostic metric is validated using laboratory experiments, the uniqueness for fault isolation is not completely evaluated. In the future, the authors aim to evaluate the effect of failure in mechanical components, such as rotor eccentricity and bearing faults, on the spectral analysis of the back-EMF.

REFERENCES

Articles

Chen, X., Hu, J., Chen, K., & Peng, Z. (2016). Modeling of electromagnetic torque considering saturation and magnetic field harmonics in permanent magnet synchronous motor for HEV. *Simulation Modelling Practice and Theory, 66*. doi:10.1016/j.simpat.2016.02.012

Cruz, S. M. A., & Cardoso, A. J. M. (2001). Stator winding fault diagnosis in three-phase synchronous and asynchronous motors, by the extended Park's vector approach. *IEEE Transactions on Industry Applications, 37*(5), 1227-1233. doi:10.1109/28.952496

Faiz, J., & Mazaheri-Tehrani, E. (2017). Demagnetization Modeling and Fault Diagnosing Techniques in Permanent Magnet Machines Under Stationary and Nonstationary Conditions: An Overview. *IEEE Transactions on Industry Applications, 53*(3), 2772-2785. doi:10.1109/TIA.2016.2608950

Faiz, J., & Nejadi-Koti, H. (2016). Demagnetization Fault Indexes in Permanent Magnet Synchronous Motors—An Overview. *IEEE Transactions on Magnetics, 52*(4), 1-11. doi:10.1109/TMAG.2015.2480379

Hendershot, J. R., & Miller, T. J. E. (2010). *Design of brushless permanent-magnet machines*: Motor Design Books.

Ilamparithi, T., & Nandi, S. (2010, 20-23 Dec. 2010). *Comparison of results for eccentric cage induction motor using Finite Element method and Modified Winding Function Approach.* Paper presented at the 2010 Joint International Conference on Power Electronics, Drives and Energy Systems & 2010 Power India.

Le Roux, W., Harley, R., & Habetler, T. (2003). *Detecting rotor faults in permanent magnet synchronous machines.* Paper presented at the 4th IEEE International Symposium on Diagnostics for Electric Machines, Power Electronics and Drives, 2003. SDEMPED 2003.

Moon, S., Lee, J., Jeong, H., & Kim, S. W. (2016). Demagnetization Fault Diagnosis of a PMSM Based on Structure Analysis of Motor Inductance. *IEEE Transactions on Industrial Electronics, 63*(6), 3795-3803. doi:10.1109/TIE.2016.2530046

Naderi, P. (2018). Magnetic-equivalent-circuit approach for inter-turn and demagnetisation faults analysis in surface mounted permanent-magnet synchronous machines using pole specific search-coil technique. *IET Electric Power Applications, 12*(7), 916-928. doi:10.1049/iet-epa.2017.0403

Park, Y., Fernandez, D., Lee, S. B., Hyun, D., Jeong, M., Kommuri, S. K., . . . Briz, F. (2019). Online Detection of Rotor Eccentricity and Demagnetization Faults in PMSMs Based on Hall-Effect Field Sensor Measurements. *IEEE Transactions on Industry Applications, 55*(3), 2499-2509. doi:10.1109/TIA.2018.2886772

Rajagopalan, S., Roux, W. l., Habetler, T. G., & Harley, R. G. (2007). Dynamic Eccentricity and Demagnetized Rotor Magnet Detection in Trapezoidal Flux

(Brushless DC) Motors Operating Under Different Load Conditions. *IEEE Transactions on Power Electronics, 22*(5), 2061-2069. doi:10.1109/TPEL.2007.904183

Saied, S., Abbaszadeh, K., & Tenconi, A. (2011). *Improvement to winding function theory for PM machine analysis*. Paper presented at the 2011 International Conference on Power Engineering, Energy and Electrical Drives.

Toliyat, H. A., Nandi, S., Choi, S., & Meshgin-Kelk, H. (2012). *Electric machines: modeling, condition monitoring, and fault diagnosis*: CRC press.

Urresty, J., Riba, J., & Romeral, L. (2013). A Back-emf Based Method to Detect Magnet Failures in PMSMs. *IEEE Transactions on Magnetics, 49*(1), 591-598. doi:10.1109/TMAG.2012.2207731

Usman, A., Joshi, B. M., & Rajpurohit, B. S. (2019, 14-17 Oct. 2019). *Modeling and Analysis of Demagnetization Faults in BLDC Motor using Hybrid Analytical-Numerical Approach*. Paper presented at the IECON 2019 - 45th Annual Conference of the IEEE Industrial Electronics Society.

Books

Lipo, T. A. (2017). *Analysis of synchronous machines*: Crc Press.